ACS APPLIED MATERIALS & INTERFACES

Research Article

www.acsami.org

Abnormal Cyclibility in Ni@Graphene Core–Shell and Yolk–Shell Nanostructures for Lithium Ion Battery Anodes

Huawei Song,[†] Hao Cui,[†,‡] and Chengxin Wang[†,*,‡]

[†]State Key Laboratory of Optoelectronic Materials and Technologies, School of Physics Science and Engineering, Sun Yat-sen (Zhongshan) University, Guangzhou 510275, People's Republic of China

[‡]The Key Laboratory of Low-Carbon Chemistry & Energy Conservation of Guangdong Province, Sun Yat-sen (Zhongshan) University, Guangzhou 510275, People's Republic of China

ABSTRACT: Electrochemical pulverization, a commonly undesirable process for durable electrodes, is reinterpreted in popular yolk–shell nanostructures. In comparison with core–shell counterparts, the yolk–shell ones exhibit enhancing ion storage and rate capability for lithium ion battery anodes. The enhancement benefits from lowered activation barriers for lithiation and delithiation, improved surfaces and interfaces for ion availability contributed by endless pulverization of active materials. By controlled etching, stable cycling with significantly improved capacity (~800 mAh g^{-1} at 0.1 A g^{-1}, 600 mAh g^{-1} at 0.5 A g^{-1}, and 490 mAh g^{-1} at 1 A g^{-1} vs 140 mAh g^{-1} at 0.1 A g^{-1}) is achieved at various rates for Ni@Graphene yolk–shell structures. Meanwhile, large rate of 20 A g^{-1} with capacity of 145 mAh g^{-1} is retained. Given initial pulverization for the activation, the tailored electrodes could stably last for more than 1700 cycles with an impressive capacity of ca. 490 mAh g^{-1} at 5 A g^{-1}. Insights into electrochemical processes by TEM and STEM reveal dispersive pulverized active nanocrystals and the intact protective graphene shells play the leading role.

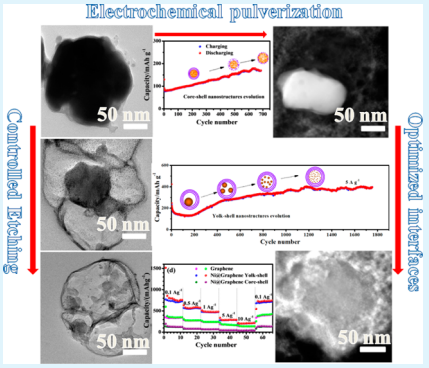

KEYWORDS: *electrochemical pulverization, Ni@Graphene, core–shell, yolk–shell, Lithium ion battery*

1. INTRODUCTION

Metal catalyzed growth of graphene has been widely applied in recent years.[1−6] Among them, graphene nanostructures evolved from phase segregation of iron, cobalt, and nickel carbides have attracted lots of interest in electrochemical fields.[3,4] The fabrication mainly involves three separate processes: the carbonization of metal particles or metal frameworks, an annealing treatment, and an etching treatment.[3] The technique, although tedious, is very popular for its availability in large scale production.[2,3]

In the field of lithium ion batteries, some potential electrode materials, e.g., silicon, germanium, and sulfur deliver unparallel ion storage capability compared with a traditional C—$LiCoO_2$ system;[7−13] however, they largely end in failure due to electrochemical pulverization and relevant exfoliation which disconnect the conductance among active materials and the current collector. To deal with this, efforts are mainly focused on the acquisition of nanoscaled active materials and embedding them in some buffering matrix.[10,14−18] These complexes have been substantiated with enhancing cycling and rate capability without compromise in capacity.[9,10,14−16,19−21]

Herein, equally satisfactory results are achieved in a different approach accompanying our reinterpretation of electrochemical pulverization. Through the "unpopular" pulverization, well-dispersive nanocrystals in intact protective graphene shells and adjustable space for buffering volume effect are simultaneously realized in common yolk–shell nanostructures. In comparison with their parent-counterparts, the technique affords full utilization of active materials and avoids the collapse of the protective layer in the meantime. Consequently, excellent electrochemical properties of large rates of 20 A g^{-1} and long lifespans of more than 1700 cycles are readily achieved with enhancing the storage capability in the electrodes.

2. EXPERIMENTAL SECTION

2.1. Synthesis of Ni@Graphene Core–Shell and Yolk–Shell Nanostructures. All the reagents were used after purchase and without purification. To attain Ni@Graphene core–shell nanostructures, nickel carbide nanoparticles are first prepared by simultaneous reduction of nickel acetate and carbonization of nickel particles in ethanol through a solvothermal method with triethylene glycol as the carbon source. Typically, 0.2 g nickel acetate tetrahydrate is dissolved into 20 mL mixture solvent of ethanol, triethylene glycol, dimethylformamide (V/V = 10:4:5); and then, the solution is transferred into Teflon-lined stainless steel autoclave (50 mL) and hydrothermally treated at 250 °C for 24 h. Ni@Graphene core–shell nanostructures could be achieved by annealing the nickel carbide particles at 500 °C for 10 min in argon atmosphere through phase segregation as reported.[3] Products in different reduction and carbonization durations are prepared for mechanism analysis. The Ni@Graphene yolk–shell nanostructures are fabricated through controlled etching of the Ni@Graphene core–shell nanostructures with diluted hydrochloride acid at 50 °C for 12 h. By adjusting the amount ratio (R = n(2HCl)/n(Ni@Graphene)) of diluted hydrochloride acid to Ni@Graphene core–shell nanostructures,

Received: May 23, 2014
Accepted: July 8, 2014
Published: July 8, 2014

 © 2014 American Chemical Society dx.doi.org/10.1021/am503016s | ACS Appl. Mater. Interfaces 2014, 6, 13765−13769

50% etched-Ni@Graphene (R = 1:2) and 80% etched-Ni@Graphene (R = 4:5) yolk−shell nanostructures are both attained for electrochemical evaluation. In calculation R, the mass of graphene is ignored.

2.2. Physiochemical Characterization. Morphologies and microstructures of the samples were characterized by thermal field emmission SEM (Quanta 400F) under 20 kV, STEM and TEM (FEI Tecnai G2 F30) under 300 kV. Structures analysis were performed by XRD (D/MAX 2200 VPC) with Cu Kα radiation scaning at 3°/min from 35° to 60°. The content of Nickel in Ni@Graphene core−shell, 50% etched-Ni@Graphene (R = 1:2) and 80% etched-Ni@Graphene (R = 4:5) yolk−shell nanostructures were indirectly determined by inductively coupled plasma-atomic emission spectrometer (ICP-AES, SPECTRO CIROS VISION). The cycled cells were also disassembled in Ar-filled glovebox. After soaking in dimethyl carbonate for 24 h, samples of the cycled electrodes were prepared for STEM and TEM characterizarion.

2.3. Electrochemical Characterization. For electrochemical characterization, electrodes were fabricated by pasting a slurry mixture of Ni@Graphene core−shell or yolk−shell nanostructures, polyvinylidene fluoride, and acetylene black with a weight ratio of 8:1:1 on copper foil by an automatic thick film coater (AFA-I). Then the coating film was desiccated in an vacuum chamber at 120 °C for 12 h. After that the foil is densified by an electromotive roller (MR-100A) and tailored to appropriate size by a coin-type cell microtome (T-06). The loadage of active materials ca. 500 μg on each piece was determined by a microbalance (d = 0.1 μg). Standard cells (CR2032) with the above tailored foils as working electrode and lithium foils as the reference and counter electrode, polypropylene micromembrane as the separator, 1 M $LiPF_6$ in ethylene carbonate (EC) and diethyl carbonate (DEC) with a weight ratio of 1:1 as the electrolyte, were assembled in an Ar-filled universal glovebox with the oxygen and water vapor pressure less than 0.3 ppm. Cyclic voltammograms were performed on an Ivium electrochemcial workstation scaning at 0.2 mV s^{-1} in a voltage cutoff of 0−3 V. For cycling and rate performance, the electrodes were galvanostatically charged and discharged in a voltage cutoff of 0.005−3 V at various rates on a mulitichannel Neware battery testing system.

3. RESULTS AND DISCUSSION

Through a modified hydrothermal approach, nickel carbide submicropowders are obtained in one step.[3] Actually, the procedure involves reduction of nickel acetate to nickel particles and the carbonization of the nickel particles to nickel carbide particles. As shown in the XRD patterns (Figure 1(a)), the evolution of nickel particles happen in less than half an hour, while the carbonization lasts more than 12 h. For the duration of 24 h, only nickel carbide exists, indicating that the nickel particles all transformed into nickel carbide particles. After a mild annealing process, nickel carbides (PDF No. 06-0697) are all transformed into metal nickel (PDF No. 65-0380) as reported previously (Figure 1(b)). Figure 2(a) exhibits the nickel carbide

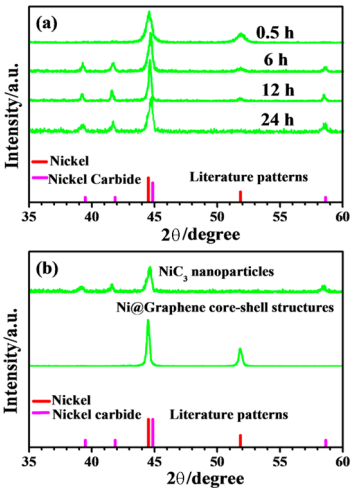

Figure 1. (a) XRD patterns for the evolution of nickel submicron particles and their carbonization in the hydrothermal process and (b) XRD patterns for the nickel carbide submicron particles and their transformation into Ni@Graphene core−shell nanostructures after annealing.

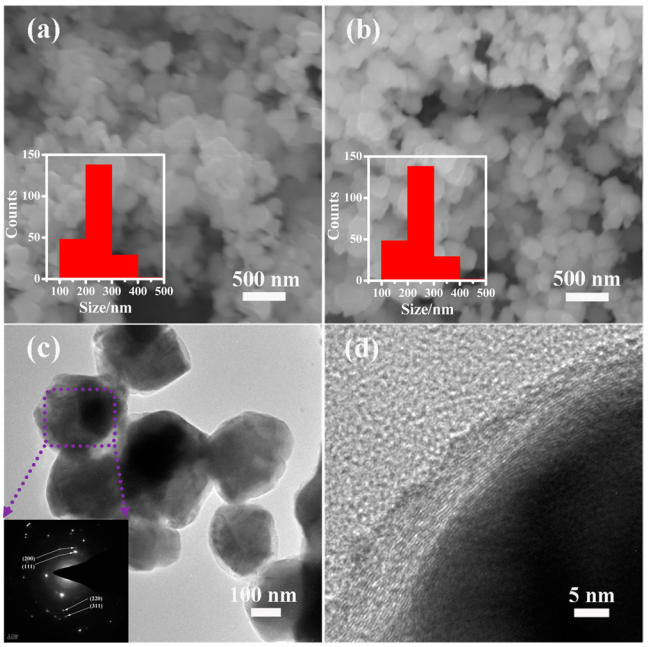

Figure 2. Microstructures for Ni@Graphene core−shell nanostructures: (a) SEM image for nickel carbide submicron particles and the bar diagram for their size evaluation (inset view); (b) SEM image for the Ni@Graphene core−shell nanostructures and the bar diagram for their size evaluation (Inset view); (c) TEM image for the Ni@Graphene core−shell nanostructures and the SAED image (inset view); and (d) HRTEM image for the Ni@Graphene core−shell nanostructure.

particles have ball-like skeletons that range from 100 to 400 nm, and most of them are 200 nm in diameter, as statistically depicted in the bar diagram (inset view of Figure 2(a)). Interestingly, these submicron particles retain their dimensions without any coalescence suffering from the annealing process (Figure 2(b) and the inset view). This implies the decarburization process for those nickel carbide particles proceeds in very short duration and the forming carbon shell efficiently inhibits further growth of those particles.

In the magnified TEM image (Figure 2(c)), sharp contrast in the particles indicates their core−shell structure, while different darkness in the cores reveals their irregularity. Moreover, the SAED image in the inset view also indicates the core is composed of several nickel crystals (PDF No. 65-0380) with different orientation well consistent with the XRD patterns. The HRTEM image (Figure 2(d)) shows the shells are graphene layers of ca. 5 nm in thickness. To evaluate the influence of shell, state-of the-art electrodes for Lithium ion battery anode are galvanostatically tested at different rates. Figure 3(a) exhibits the electrodes deliver poor Li^+ storage capability with capacity less than 150 mAh g^{-1} at 0.1 A g^{-1}. However, the core−shell nanostructure exhibits enhancing cyclibility for the long-term test at 0.5 A g^{-1}(Figure 3(b)). The enhancement may be attributed to pulverization of active materials in the cores, which have improved the ion availability of the electrode through enlarging

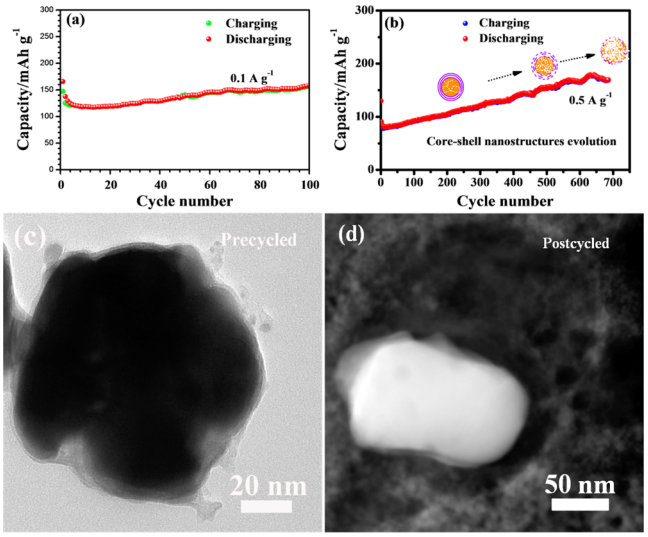

Figure 3. Electrochemical characterization for the Ni@Graphene core–shell nanostructures: (a) cycling performance tested at 0.1 A g^{-1}; (b) long-term test cycled at 0.5 A g^{-1} and the schematic illustration for the evolution of the core–shell nanostructure during cycling; (c) intact Ni@Graphene core–shell nanostructure before cycled; (d) Ni@Graphene core–shell nanostructure after tested for 700 cycles with collapsed graphene shell.

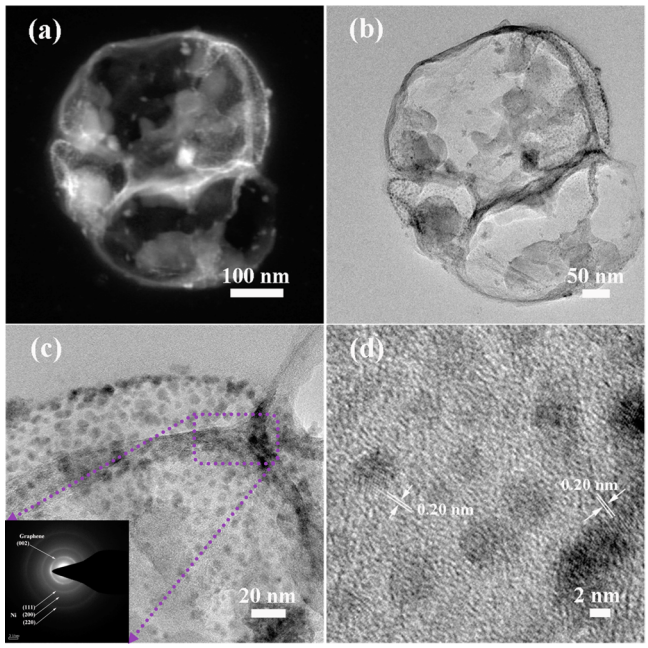

Figure 4. Microstructures for the 80% etched Ni@Graphene nanostructures: (a) STEM image; (b) and (c) TEM images in different magnification with SAED image in the inset view of (c); and (d) HRTEM image with well crystallized nickel nanocrystals.

interfaces and surfaces among the active cores. As the test lasts, this enhancement fails for the collapse of the protective graphene shells, which might be caused by volume effect common in conversion type electrodes. This may be verified by the breakage of the intact graphene shell in the Ni@Graphene core–shell electrode (Figure 3(c),(d)).

To alleviate the volume effect, the 80% etched Ni@Graphene yolk–shell nanostructures are fabricated. As shown in the STEM and TEM images (Figure 4(a),(b)), the nanostructures retain the intact graphene shells, while the cores are substituted by nanoparticles anchored in the inner surfaces of the graphene shell. The magnified TEM image, the SAED rings, and the HRTEM image (Figure 4(c),(d)) also substantiate the nanoparticles are Ni nanoparticles (PDF No. 65-0380) with a size less than 5 nm. The reduced size for Ni particles and the large space in the shells not only improved the ion availability, but also severely lower the activation barrier for the electrochemical process. As depicted in the cyclic voltammogram (CV) (Figure 5(a)), both of the first cathode scans of the core–shell and yolk–shell structures are characteristic of two marked peaks ascribed to the formation of solid electrolyte interphase above 1 V and the formation Li_2O between 0.5 and 1 V and gentle slope near 0 V attributed to lithiation of graphene, while the peaks centered at 0.5, 1.2, and 2.4 V in the anodes scans are respectively ascribed to the delithiation of graphene, the formation of nickel oxide and the delithiation of some interfacial storage effect.[10,22,23] Evidently, the marked peak shift toward lower voltage in the cathode scans, the intensified peaks for delithiation of graphene and nickel oxidation, and the enhanced interfacial storage in the anode scans all substantiated the improved interfaces and lowered activation barriers due to the controlled etching. Moreover, the enhanced ion storage capability for yolk–shell nanostructures comparing with the core–shell nanostructures is intuitively embodied in the typical charge–discharge curves (Figure 5(b)) covering three components: ion storage in graphene, redox of Ni nanocrystals, and charge storage among the interfaces.[14] This verified that ion storage capability and interfaces improvement are simultaneously realized through transformation from core–shell to yolk–shell nanostructures.

Consequently, both cycling and rate performance are readily improved. Figure 5(c) exhibits the yolk–shell nanostructures deliver large capacity of ca. 800, 600, and 490 $mAhg^{-1}$ at 0.1, 0.5, and $1Ag^{-1}$ respectively. Moreover, the impressive storage capability lasts for more than 100 cycles without any decay. Except for the stable cycling, the rate performance is also well elevated. As depicted in Figure 5(c), suffering from successive altering rates ranging from 0.1 to 20 A g^{-1}, the yolk–shell nanostructures retain 145 mAh g^{-1} at 20 A g^{-1}. When the rate returns to 0.1 A g^{-1}, a large reversible capacity near 800 mAh g^{-1} is recovered. To gain insights into the improved ion storage capability and rate performance, we try to figure out the contribution each component in those nanostructures. In consideration of nickel content indirectly determined by ICP as 98.4% and 88.4%, the theoretical capacity (743 × wt $\%_{Ni}$ + 380 × wt $\%_{Graphene}$, the theoretical capacity of Ni as 743 mAh g^{-1} and measured capacity of as prepared graphene as 380 mAh g^{-1}) should be about 742 mAh g^{-1} and 693 mAh g^{-1} for the Ni@Graphene core–shell and yolk–shell nanostructures, respectively. This indicates that most nickel in the core–shell structures are electrochemically inactive, well consistent with the mentioned CV result. As for the yolk–shell structure, the capacity gap between the theoretical and the measured verifies the existence of another approach contribution to the improved ion storage capability like interfacial storage effect. Besides, the STEM image (Figure 5(e)) for the postcycled electrode reveals intact protective layer and well dispersive active material particles are fairly retained for 100 cycles. This verifies the etching process plays an important role in the electrochemical improvement.

Although the 80% etched Ni@Graphene nanostructures significantly improved the electrochemical properties, yet the

dx.doi.org/10.1021/am503016s | ACS Appl. Mater. Interfaces 2014, 6, 13765–13769

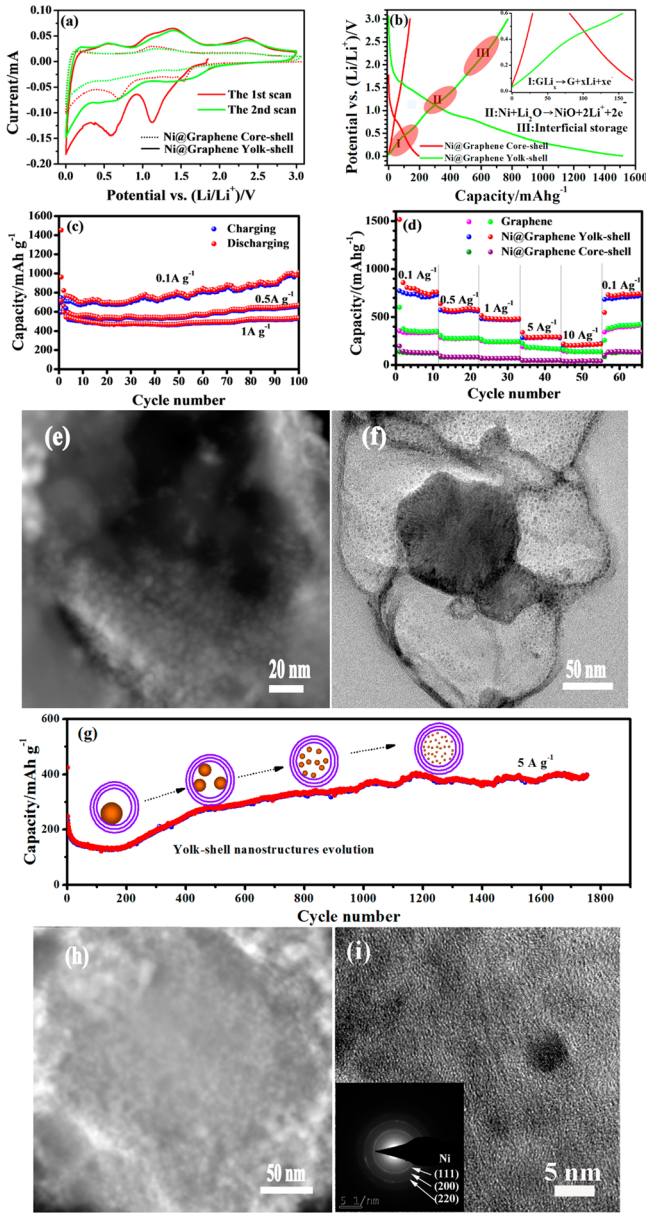

Figure 5. Electrochemical characterization for the etched Ni@Graphene nanostructures: (a) cyclic voltammograms and (b) typical charge−discharge curves for the 80% etched Ni@Graphene nanostructures in comparison with that of the core−shell nanostructures, inset view of (b) is the locally magnified curves indicating delithiation of graphene and the colored ellipse shows different dilithiation processes; (c) cycling performance for the 80% etched Ni@Graphene nanostructures tested at different rates; (d) rate performance for the 80% etched Ni@Graphene nanostructures tested at variable rates ranging from 0.1 A g^{-1} to 20 A g^{-1} comparing with fully etched graphene balls and Ni@Graphene core−shell nanostructures; (e) STEM image for the cycled 80% etched Ni@Graphene nanostructure; (f) TEM image for the 50% etched Ni@Graphene yolk−shell nanostructure; (g) cycling performance for the 50% etched Ni@Graphene nanostructures tested at 5 A g^{-1} and the schematic illustration for the evolution of the yolk−shell nanostructure during cycling; (h) STEM image for cycled 50% etched Ni@Graphene yolk−shell nanostructure; and (i) HETEM image for the cycled 50% etched Ni@Graphene yolk−shell nanostructure and its SAED image (inset view).

loss of active Ni weakens the utility. In order to fully utilize the active Ni, a reduction of the etching depth is easily expected. However, the unknown feasibility for activating the large Ni particles and the dispersion of the active Ni during the cycling challenge this attempt. Hence, electrodes composed of the 50% etched Ni@Graphene yolk−shell nanostructures are fabricated (the content of nickel as 95.7% determined by ICP) and the size of nickel is reduced to less than 100 nm (Figure 5(f)). Figure 5(g) shows the electrode exhibits enhancing cyclibility with capacity of ca. 490 mAh g^{-1} at 5Ag^{-1} as the test lasts for more than 1700 cycles. Specifically, the cycling could be divided into two stages: the initial several hundred cycles for pulverization of the Ni core and the stable cycling state. Comparing the morphology of the precycled nanostructures with that of the postcycled one (Figure 5(f),(h)), bump Ni core ca. 100 nm is thoroughly pulverized into Ni nanocrystals less than 5 nm with well dispersion in the STEM and HRTEM images (Figure 5(h),(i)).

The fairly good dispersion of core species suffering from initial electrochemical pulverization confirms that optimizing electrochemical properties could be readily obtained through adjusting the core−shell structures. By varying the size of the core, an adjustable space in the shell for buffering volume effect would be achieved, while engineered interfaces among the active species would be evolved, benefiting by the electrochemical pulverization. This provides us with a facile approach to utilize electrochemical pulverization in a controlled manner in some special configurations.

4. CONCLUSIONS

In summary, Ni@Graphene core−shell nanostructures are fabricated by annealing the nickel carbide nanoparticles achieved through the reduction and carbonization of nickel acetate in hydrothermal process. The core−shell nanostructures exhibit poor electrochemical properties due to their initially large activation barrier and final collapse of graphene shells, while stable cycling, enhancing storage, and rate capability are simultaneously acquired in yolk−shell nanostructures obtained with a controlled etching process. The adjustable space in the yolk−shell accommodates good dispersion of pulverized active nanocrystals and the retention of intact protective graphene layer which finally contribute to the significantly improved cyclibility. Besides, the utilization of electrochemical pulverization in a controlled manner is also applicable to a variety of fields, such as lithium−sulfur batteries, sodium-ion batteries, fuel cells, and so forth.

AUTHOR INFORMATION

Corresponding Author

*Tel/Fax: +86-20-84113901; e-mail: wchengx@mail.sysu.edu.cn.

Notes

The authors declare no competing financial interest.

ACKNOWLEDGMENTS

This work was financially supported by the National Natural Science Foundation of China (Nos. 51125008 and 11274392).

REFERENCES

(1) Kim, H. J.; Wen, Z. H.; Yu, K. H.; Mao, O.; Chen, J. H. Straightforward Fabrication of a Highly Branched Graphene Nanosheet Array for a Li-ion Battery Anode. *J. Mater. Chem.* **2012**, *22*, 15514−15518.

(2) Xiao, X.; Michael, J. R.; Beechem, T.; McDonald, A.; Rodriguez, M.; Brumbach, M. T.; Lambert, T. N.; Washburn, C. M.; Wang, J.; Brozik, S. M.; Wheeler, D. R.; Burckel, D. B.; Polsky, R. Three

Dimensional Nickel−Graphene Core−Shell Electrodes. *J. Mater. Chem.* **2012**, *22*, 23749−23754.
(3) Yoon, S. M.; Choi, W. M.; Baik, H.; Shin, H. J.; Song, I.; Kwon, M. S.; Bae, J. J.; Kim, H.; Lee, Y. H.; Choi, J. Y. Synthesis of Multilayer Graphene Balls by Carbon Segregation from Nickel Nanoparticles. *ACS Nano* **2012**, *6*, 6803−6811.
(4) Chiang, R. T.; Chiang, R. K.; Shieu, F. S. Preparation of Non-spherical Hollow Carbon Nanocapsules from Nickel Nanoprecursors. *Solid State Sci.* **2012**, *14*, 1221−1225.
(5) Li, N.; Song, H.; Cui, H.; Wang, C. Sn@Graphene Grown on Vertically Aligned Graphene for High-Capacity, High-Rate, and Long-Life Lithium Storage. *Nano Energy* **2014**, *3*, 102−112.
(6) He, C.; Wu, S.; Zhao, N.; Shi, C.; Liu, E.; Li, J. Carbon-Encapsulated Fe_3O_4 Nanoparticles as a High-Rate Lithium Ion Battery Anode Material. *ACS Nano* **2013**, *7*, 4459−4469.
(7) Pang, C.; Cui, H.; Yang, G.; Wang, C. Flexible Transparent and Free-Standing Silicon Nanowires Paper. *Nano Lett.* **2013**, *13*, 4708−4714.
(8) Jin, S.; Li, N.; Cui, H.; Wang, C. Growth of the Vertically Aligned Graphene@ Amorphous GeO_x Sandwich Nanoflakes and Excellent Li Storage Properties. *Nano Energy* **2013**, *2*, 1128−1136.
(9) Song, H.; Li, N.; Cui, H.; Wang, C. Enhanced Capability and Cyclability of SnO_2-Graphene Oxide Hybrid Anode by Firmly Anchored SnO_2 Quantum Dots. *J. Mater. Chem. A* **2013**, *1*, 7558−7562.
(10) Song, H.; Yang, G.; Cui, H.; Wang, C. Electrodes Engineering of High Power, Long Life and Excellent Cycling Stability for Rechargeable Lithium Batteries. *Nano Energy* **2014**, *3*, 16−25.
(11) Li, N.; Jin, S.; Liao, Q.; Cui, H.; Wang, C. X. Encapsulated within Graphene Shell Silicon Nanoparticles Anchored on Vertically Aligned Graphene Trees as Lithium Ion Battery Anodes. *Nano Energy* **2014**, *5*, 105−115.
(12) Wei Seh, Z.; Li, W.; Cha, J. J.; Zheng, G.; Yang, Y.; McDowell, M. T.; Hsu, P. C.; Cui, Y. Sulphur−TiO_2 Yolk−Shell Nanoarchitecture with Internal Void Space for Long-Cycle Lithium−Sulphur Batteries. *Nat. Commun.* **2013**, *4*, 1331.
(13) Ji, L.; Zheng, H.; Ismach, A.; Tan, Z.; Xun, S.; Lin, E.; Battaglia, V.; Srinivasan, V.; Zhang, Y. Graphene/Si Multilayer Structure Anodes for Advanced Half and Full Lithium-Ion Cells. *Nano Energy* **2012**, *1*, 164−171.
(14) Song, H.; Li, N.; Cui, H.; Wen, X.; Wei, X.; Wang, C. Significantly Improved High-Rate Li-Ion Batteries Anode by Encapsulating Tin Dioxide Nanocrystals into Mesotunnels. *CrystEngComm* **2013**, *15*, 8537.
(15) Shen, L.; Song, H.; Cui, H.; Wen, X.; Wei, X.; Wang, C. Fe_3O_4-Carbon Nanocomposites via a Simple Synthesis as Anode Materials for Rechargeable Lithium Ion Batteries. *CrystEngComm* **2013**, *15*, 9849−9854.
(16) Yang, G.; Cui, H.; Yang, G.; Wang, C. Self-Assembly of $Co_3V_2O_8$ Multilayered Nanosheets: Controllable Synthesis, Excellent Li-Storage Properties, and Investigation of Electrochemical Mechanism. *ACS Nano* **2014**, *8*, 4474−4487.
(17) Shen, L.; Wang, C. Hierarchical Co_3O_4 Nanoparticles Embedded in a Carbon Matrix for Lithium-Ion Battery Anode Materials. *Electrochim. Acta* **2014**, *133*, 16−22.
(18) Jin, S.; Wang, C. Synthesis and First Investigation of Excellent Lithium Storage Performances of Fe_2GeO_4/Reduced Graphene Oxide Nanocomposite. *Nano Energy* **2014**, *7*, 63−71.
(19) Yang, G. Z.; Song, H. W.; Cui, H.; Liu, Y. C.; Wang, C. X. Ultrafast Li-ion Battery Anode with Superlong Life and Excellent Cycling Stability from Strongly Coupled ZnO Nanoparticle/Conductive Nanocarbon Skeleton Hybrid Materials. *Nano Energy* **2013**, *2*, 579−585.
(20) Song, H.; Li, N.; Cui, H.; Wang, C. Monodisperse SnO_2 Nanocrystals Functionalized Multiwalled Carbon Nanotubes for Large Rate and Long Lifespan Anode Materials in Lithium Ion Batteries. *Electrochim. Acta* **2014**, *120*, 46−51.
(21) Wu, Z. S.; Zhou, G. M.; Yin, L. C.; Ren, W. C.; Li, F.; Cheng, H. M. Graphene/Metal Oxide Composite Electrode Materials for Energy Storage. *Nano Energy* **2012**, *1*, 107−131.
(22) Poizot, P.; Laruelle, S.; Grugeon, S.; Dupont, L.; Tarascon, J. M. Nano-Sized Transition-Metal Oxides as Negative-Eectrode Materials for Lithium-Ion Batteries. *Nature* **2000**, *407*, 496−499.
(23) Poizot, P.; Laruelle, S.; Grugeon, S.; Tarascon, J. M. Rationalization of the Low-Potential Reactivity of 3D-Metal-Based Inorganic Compounds toward Li. *J. Electrochem. Soc.* **2002**, *149*, A1212−A1217.